Available online at www.sciencedirect.com
SCIENCE DIRECT®
Computer Physics Communications 153 (2003) 179–189
Computer Physics Communications
www.elsevier.com/locate/cpc

A parallel Beowulf-based system for the detection of gravitational waves in interferometric detectors

P. Amico [a,b], L. Bosi [a,b], C. Cattuto [a,b], L. Gammaitoni [a,b], F. Marchesoni [a,c], M. Punturo [a,*], F. Travasso [a,b], H. Vocca [a,b]

[a] *Istituto Nazionale di Fisica Nucleare, Sezione di Perugia, VIRGO Project, I-06100 Perugia, Italy*
[b] *Dipartimento di Fisica, Universita' di Perugia, I-06100 Perugia, Italy*
[c] *Dipartimento di Fisica, Universita' di Camerino, I-62032 Camerino, Italy*

Received 25 November 2002; accepted 24 February 2003

Abstract

The detection, in a modern interferometric detector like Virgo, of a gravitational wave signal from a coalescing binary stellar system is an intensive computational task both for the *on-line* and *off-line* computer systems. A parallel computing scheme using the Message Passing Interface (MPI) is described. Performance results on a small scale cluster are reported.

PACS: 04.80.N; 95.55.Y; 07.05; 89.80

Keywords: Gravitational waves; Beowulf clusters; Message passing; Coalescing binaries; Virgo

1. Introduction

One of the most interesting predictions of Einstein's theory of general relativity is the existence of gravitational waves. The wave equation for *space–time* was proposed by Einstein in 1916, but no direct evidence has yet been observed. An indirect detection of gravitational radiation, obtained by monitoring the orbital period decay of the binary system 1913+16 resulted in the Nobel prize for Russel Hulse and Joseph Taylor [1] in 1993.

The first experiment aimed at detecting gravitational waves directly was performed by Joseph Weber [2], in the 60s, using a room temperature resonant bar detector. Following this pioneering work, several generations of improved resonant detectors have been developed by decreasing the operating temperature down to few milliKelvin [3] in order to minimize thermal noise and by using very low noise transducers like SQUIDs. A gravitational wave interacting with a bar detector excites the fundamental longitudinal mechanical mode. The *resonant* nature of this kind of detector limits its bandwidth to a few Hz around a typical resonant frequency of about 1 kHz, where the response of the instrument is highest.

Recently, a new family of detectors has been developed: interferometric detectors. In this case, a Michelson interferometer is set up with arms a few kilometers long that typically are optically multiplied in

* Corresponding author.
E-mail address: michele.punturo@pg.infn.it (M. Punturo).

0010-4655/03/$ – see front matter
doi:10.1016/S0010-4655(03)00223-6

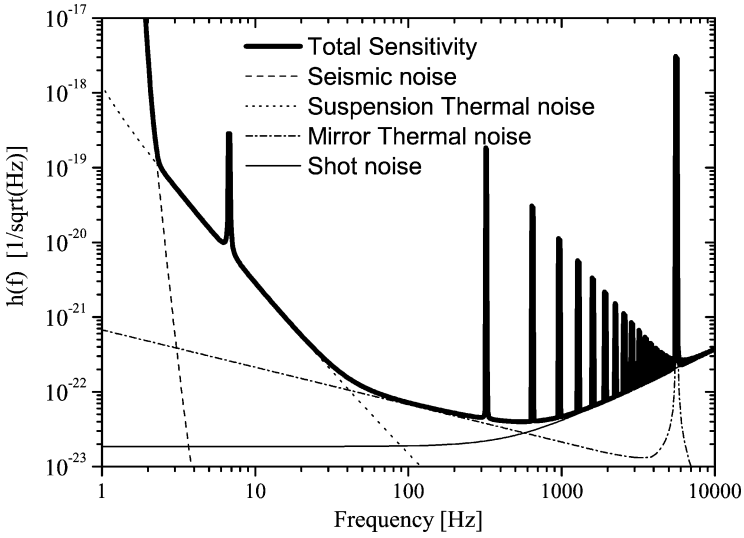

Fig. 1. Virgo Sensitivity curve; the total sensitivity (continuous tick line) is reported together with the main noise contributions: seismic noise (dashed line), suspension thermal noise (dotted line), mirror thermal noise (dash-dotted line) and laser shot noise (continuous thin line).

length by using Fabry–Perot cavities. Optical components (mirrors) are suspended to realize a set of *free falling* reference masses that—ideally—are only perturbed by their interaction with gravitational waves (GW). Because of the tidal nature of GWs, the length of the interferometer arms are modulated by the passage of a gravitational wave which produces a signal at the output of the interferometer. Several detectors of this kind are under construction, or have just become operative: LIGO [4] in the USA, Geo600 [5] in Germany, Tama [6] in Japan and Virgo [7] in Italy. Interferometric detectors have a very large spectral sensitivity bandwidth compared to resonant detectors. Specifically, Virgo—with a high performance superattenuator seismic isolation system [8] and a low thermal noise pendulum suspension [9]—will show the largest frequency bandwidth, ranging from a few Hz up to few kHz [10] (see Fig. 1). Later in this paper, it will be shown how the wide spectral sensitivity bandwidth is closely linked to the computational cost of GW signal detection.

2. Gravitational waves

In this section, a short summary of the physics of gravitational waves is presented. Given the vastness of the argument, such an discussion has to be very limited. For more thorough accounts, refer to the references.

Einstein's equations of General Relativity

$$G_{\mu\nu} = \frac{8\pi G}{c^4} T_{\mu\nu}, \tag{1}$$

link the energy-momentum tensor $T_{\mu\nu}$, source of the space–time curvature, to the curvature itself, described by the Einstein tensor $G_{\mu\nu}$

$$G_{\mu\nu} = R_{\mu\nu} - \tfrac{1}{2} g_{\mu\nu} R. \tag{2}$$

Here G is the universal gravitational constant, c the speed of light, $R_{\mu\nu}$ the Ricci's tensor, R the curvature scalar and $g_{\mu\nu}$ is the generic space–time metric tensor. In a weak field approximation, for example, far away from GW sources, it is possible to treat the curvature of the space–time as a perturbation, and to linearize Eq. (1). In this linear approximation, the metric tensor $g_{\mu\nu}$ becomes

$$g_{\mu\nu} = \eta_{\mu\nu} + h_{\mu\nu}, \tag{3}$$

where $\eta_{\mu\nu}$ is the metric tensor of flat (Minkowski) space and $h_{\mu\nu}$ represents the "ripples" on the otherwise flat space–time due to traveling gravitational waves. In the absence of mass, the perturbation $h_{\mu\nu}$ obeys the following linear wave equation:

$$\left(-\frac{\partial^2}{\partial t^2} + \nabla^2\right) h_{\mu\nu} = 0. \tag{4}$$

For the specific case of a monochromatic wave traveling along the z direction, and by choosing a suitable gauge (Transverse Traceless gauge), the metric perturbation $h_{\mu\nu}$ can be written as

$$h_{\mu\nu} = \begin{pmatrix} 0 & 0 & 0 & 0 \\ 0 & h_+ & h_\times & 0 \\ 0 & h_\times & h_+ & 0 \\ 0 & 0 & 0 & 0 \end{pmatrix} e^{i(\Omega t - kz)}, \tag{5}$$

where Ω is the wave frequency, and h_+ and $h_\times$ are two independent polarization states of the traveling wave. The effect of this perturbation on a ring of matter located in a plane perpendicular to the propagation direction of a "+" polarized wave is a quadrupolar deformation, as suggested by the invariant distance equation:

$$\begin{aligned} ds^2 &= g_{\mu\nu}\,dx^\mu\,dx^\nu = d(ct)^2 - (1+h_+)\,dx^2 \\ &\quad - (1-h_+)\,dy^2 - dz^2. \end{aligned} \tag{6}$$

3. Astrophysical sources

Einstein showed how the generation of gravitational waves is related to the presence of a source mass distribution with quadrupolar moment Q_{ij}

$$Q_{ij} = \int_V \rho\left(x_i x_j - \tfrac{1}{3}\delta_{ij} r^2\right) dV \tag{7}$$

through the second derivative of the quadrupolar moment itself

$$h_{ij} = \frac{2G}{Rc^4}\ddot{Q}_{ij}. \tag{8}$$

Thus, the amplitude of a remotely-generated space–time perturbation depends on the asymmetry of the source mass distribution, on the amount of mass involved, on the detailed time-dependence of the process, and on the distance from the source to the observer. Because of the weak coupling between GWs and matter, as suggested by Eq. (1) ($\frac{8\pi G}{c^4} \simeq 2\times 10^{-43}$) the typical perturbation expected on Earth due to an astrophysical event is no larger than $h \simeq 10^{-21}$.

Several astrophysical systems and phenomena are potential candidate sources of gravitational waves [11]: aspheric supernovae explosions, rotating neutron stars, background noise of cosmological origin, inspiralling binary stellar systems. In this paper, only the last type of source will be considered.

Two stars composing a close binary system radiate orbital energy in the form of gravitational waves. As the stellar system loses energy, the stars get closer and closer, and their orbital period becomes shorter and shorter, until a catastrophic event occurs—called "collapse"—which terminates the individual existence of the stars. The ensuing strong emission of gravitational radiation is an interesting candidate for experimental observation by interferometric GW detectors. Long before the collapse, the motion of the stars in binary system can be described by using a Newtonian approach, yielding the time evolution of the orbital frequency,

$$\omega(t) = \frac{1}{4}\left[\frac{(G\widetilde{M})^{5/3}}{5c^5}\right]^{-3/8}(t_c - t)^{-3/8}, \tag{9}$$

where $\widetilde{M}$ is the so-called "chirp mass" (related to the reduced mass μ of the binary system and to its total mass M_T by $\widetilde{M} = \mu^{3/5}M_T^{2/5}$), and t_c is the time at which coalescence occurs. The amplitudes of the two wave polarizations are:

$$\begin{aligned} h_+(t,R,i) &= 4\frac{1+(\cos i)^2}{2}\frac{(G\widetilde{M})^{5/3}}{Rc^4} \\ &\quad \cdot \omega^{2/3}(t)\cdot\cos\big(2\omega(t)t\big), \\ h_\times(t,R,i) &= 4(\cos i)\frac{(G\widetilde{M})^{5/3}}{Rc^4}\cdot\omega^{2/3}(t)\cdot\sin\big(2\omega(t)t\big), \end{aligned} \tag{10}$$

where R is the distance of the binary system and i is the angle of the binary axis with respect to the line of sight. Inserting into Eq. (10) typical values for the physical parameters (single star mass of about 1.4 solar masses, distance of about 10 Mpc and orbital frequency of a few hundred Hz, close to coalescence) it is possible to estimate the wave amplitude mentioned above, on the order of 10^{-21}.

Terrestrial gravitational wave detectors, like Virgo, aim at detecting the gravitational radiation emitted close to coalescence, because the expected signal is strongest at that time. In this regime, the Newtonian approximation for the orbital motion of the binary system is no longer valid, and non-Newtonians corrections must be introduced. The typical formalism adopted to address this issue is the so-called *post-Newtonian* (PN) approximation: it is a perturbative approach in which the expansion parameter is $\sqrt{v/c}$, where v is the source speed. Several orders of PN approximation have been computed [12,13], going up to

the third order [14]. Up to the second PN order, neglecting the contributions due to star spin, the wave amplitude can be expressed as

$$h_{+,\times} = \frac{2G\mu}{c^2 R}\left(\frac{GM_T}{c^3}\omega\right)\left(H^{(0)}_{+,\times} + \xi^{1/2}H^{(1/2)}_{+,\times} + \xi^{1}H^{(1)}_{+,\times} + \xi^{3/2}H^{(3/2)}_{+,\times} + \xi^{2}H^{(2)}_{+,\times}\right), \quad (11)$$

where

$$\xi = \left(\frac{GM_T}{c^3}\omega(t)\right)^{2/3}, \quad (12)$$

and $H^{(pn)}_{+,\times}$ are functions of the star masses, of the angle i and of time t.

4. Signal detection

The small space–time ripple due to the gravitational wave produces a tiny variation ΔL of the interferometer optical length, $\Delta L/L_0 \simeq h/2$. For an interferometer with $L_0 = 3$ km, like Virgo, the effective displacement is of the order of $\Delta L \simeq 10^{-18}$ m. Thus, it is evident that signal detection in this kind of detector is a typical problem of signal extraction from a noisy time series of data.

Let us suppose that the output signal of the interferometer can be described as the time series

$$x(t) = m(t) + n(t), \quad (13)$$

where $m(t)$ is the signal and $n(t)$ is a noise background (due to both gravitational radiation and the detector itself). To successfully detect the signal $m(t)$, This noisy series must be filtered in such a way to maximize the signal-to-noise ratio at the output of the filter itself. A generic linear filter $\widehat{K}$ applied to the time series $x(t)$ transforms each component in the following way,

$$y(t) = \widehat{K}\big[x(t)\big] = \widehat{K}\big[m(t)\big] + \widehat{K}\big[n(t)\big] = \mu(t) + \nu(t), \quad (14)$$

and using the convolution theorem, it is possible to write

$$\mu(t) = \frac{1}{2\pi}\int_{-\infty}^{+\infty} \mathrm{e}^{\mathrm{i}\omega t} K(\omega) M(\omega)\,\mathrm{d}\omega,$$

$$\nu(t) = \frac{1}{2\pi}\int_{-\infty}^{+\infty} \mathrm{e}^{\mathrm{i}\omega t} K(\omega) N(\omega)\,\mathrm{d}\omega. \quad (15)$$

Here the capital letters indicate the Fourier transforms of the time series and of the filter impulsive response $k(t)$. The average power at the output of the filter, due to the noise only, is

$$\big\langle \nu^2(t)\big\rangle = \frac{1}{2\pi}\int_{-\infty}^{+\infty} \big|K(\omega)\big|^2 S_n(\omega)\,\mathrm{d}\omega, \quad (16)$$

where $S_n(\omega)$ is the noise power spectrum. The signal to noise ratio (SNR) ρ can be defined as

$$\rho^2 = \frac{\mu^2(t_0)}{\langle \nu^2(t)\rangle} = \frac{1}{2\pi}\frac{\left|\int_{-\infty}^{+\infty} \mathrm{e}^{\mathrm{i}\omega t} K(\omega) M(\omega)\,\mathrm{d}\omega\right|^2}{\int_{-\infty}^{+\infty} |K(\omega)|^2 S_n(\omega)\,\mathrm{d}\omega}. \quad (17)$$

Assuming that the noise is Gaussian and stationary, it is possible to find the optimal filter $K(\omega)$ that maximizes the SNR: the Wiener filter [15], or *matched* filter:

$$K_{\mathrm{opt}}(\omega) = k_0 \mathrm{e}^{-\mathrm{i}\omega t_0}\frac{M(\omega)^*}{S_n(\omega)}. \quad (18)$$

The output of such optimal filter is

$$y_{\mathrm{opt}}(t - t_0) = \frac{k_0}{2\pi}\int_{-\infty}^{+\infty} \frac{M^*(\omega)X(\omega)}{S_n(\omega)}\mathrm{e}^{\mathrm{i}\omega(t-t_0)}\,\mathrm{d}\omega, \quad (19)$$

and by using the transfer function $K_{\mathrm{opt}}(\omega)$, the maximum value of the SNR can be computed as

$$\rho^2 = \frac{1}{2\pi}\int_{-\infty}^{+\infty} \frac{|M(\omega)|^2}{S_n(\omega)}\,\mathrm{d}\omega. \quad (20)$$

If the noise is white ($S_n(\omega) = S_0$), the SNR acquires the meaning of ratio between energy of the signal and power of the noise $\rho^2 = E_x^2/S_0$, and the output of the filter is

$$y_{\mathrm{opt}}(t - t_0) = \frac{k_0}{2\pi S_0}\int_{-\infty}^{+\infty} M^*(\omega)X(\omega)\mathrm{e}^{\mathrm{i}\omega(t-t_0)}\,\mathrm{d}\omega \propto \int_{-\infty}^{+\infty} x(\tau)m(t+\tau+t_0)\,\mathrm{d}\tau, \quad (21)$$

that is the time correlation between the input data series and the expected signal.

From Eqs. (18) and (20) it is clear that to build the optimal filter, it is necessary to know the shape of the signal mixed with the noise (but not its amplitude). For coalescing binaries, the shape of the expected signal is known in a parametric form, up to the chosen post-Newtonian approximation. From Eqs. (10) and (11), neglecting the role of the angle i, the only parameters affecting the signal shape are the star masses (in Eq. (10) the chirp mass only). For this reason the coalescing binaries are called *standard candles*: both the distance of the source and its red-shift can be extracted from the waveform. The masses of the coalescing stars are unknown parameters; since it is impossible to apply to the data stream coming from the detector a Wiener filter corresponding to each pair of star masses, it is necessary to use a grid of possible signal candidates, called *templates*. The mismatching between the masses used to compute the template and the actual physical masses decreases the SNR, because of the sub-optimality of mismatched filtering. A grid of templates must be built, where the distance between the grid nodes is chosen to accommodate an acceptable SNR loss. The number of templates in the grid is then defined by the distance in the parameters space (a two-dimensional space in the second PN approximation) and the selected lower and upper boundaries for star masses.

5. Template construction

In order to build the template grid, it is first necessary to define precisely the characteristics and size of the templates. From Eqs. (9) and (10), it follows that, far from coalescence, the orbital frequency is small and consequently the signal amplitude is also small. At low frequencies, the sensitivity of Virgo (see Fig. 1) is limited by the seismic noise and by the thermal noise of the suspension system. Because of this, it is possible to remove the low frequency component of the templates, losing only a negligible fraction of the corresponding SNR. Hence, the length of templates, in time, is limited by the chosen cut-in frequency.

In the previous section, the detection theory has been introduced for the case of time-continuous signals. In reality, the Virgo data acquisition system samples the output of the interferometer at 20 kHz and, thus, discrete-time analysis tools must be adopted. In this scenario, the required size of a template (measured as the number of discrete points that it is composed of) is determined by the sampling frequency used for the signal processing. Prior to the last stable orbit, the main spectral content of a coalescence signal is under 1 kHz; it is thus possible to downsample the data stream at the output of the interferometer without significantly affecting the signal detection efficiency (SNR). The choice of the downsampled frequency on one side, and of the cut-in frequency on the other, define the computational cost of signal processing for detection. In the case of Virgo, such a cost is higher than for other detectors, because its higher sensitivity at low frequencies allows a lower cut-in frequency, significantly increasing the SNR.

Choosing $0.9 \div 2.0$ solar masses as boundary for the template space generation, 30 Hz as lower cut-in for the templates (corresponding to about 100 s of template length) and a downsampled frequency of 2048 Hz, it is possible to build a 45,000 templates grid (taking in account the two polarizations of the gravitational wave) loosing only about 3% in terms of SNR [16]. From Eq. (10) (or Eq. (11)), it is clear that the largest signals are expected from the most massive stars. Thus, the best candidates are coalescing binaries of neutron stars and black holes. The above mass interval, selected to compute the templates grid, is compatible with a binary system formed by neutron stars, but not by black holes. The heavier the binary system is, the shorter (in time) is the corresponding template, so that the largest computational load is due to the lightest pairs of stars.

From Eq. (21), it is evident that the matched filter can be implemented in the time as well as in the frequency domain. In time, the computational cost of the correlator is given by $2N^2$, where N is the number of data points. In the frequency domain, by using the FFT algorithm to transform the signal, the computational cost grows as $12N \log_2 N$, and for large enough, N, the second method is more efficient [17].

It now possible to determine the required size of the data buffer and of the templates used to compute the matched filter. Since neither the templates or the interferometer output is a periodic signal, *zero-padding* [17] of the templates is necessary in order to avoid edge effects in computing the correlator. This doubles their length from about 100 to 200 s, corre-

sponding to 409,600 data points for the sampling frequency mentioned above. Since the FFT algorithm requires a number of data points which is an integer power of 2, an effective length of 524,288 is needed for both the data buffer and the templates, corresponding to 256 s of interferometer output. Finally, since double precision floating numbers are used, the in-memory size of the data buffer and of each template is about 4 MB.

6. Hardware and software environment

In the previous section, it was shown that about 45,000 matched filters of 4 MB each must be computed to search for a coalescing binary signal in the output of the Virgo gravitational wave detector. Once each filter has been computed, it is necessary to compare its maximum output against a predefined threshold, chosen according to a false alarm rate that is regarded as acceptable (Neyman–Person criterion [18]). Given that the detector is operating continuously, an *in-time* detection strategy has to be implemented, maintaining the data analysis at about the same speed as data acquisition. Hence, all of the 45,000 templates must be matched in 256–100 seconds: an *in-time* processing scheme must compute about $45{,}000/150 = 300$ templates per second, keeping in memory about $45{,}000 \times 4\,\text{MB} = 180$ GBytes of data. It is clear that the required computational power is quite significant, and that the need arises for either a supercomputer or a cluster of PCs.

The cluster solution was investigated, implementing a few Beowulf clusters (see http://www.beowulf.org) of personal computers. Mainly, an older cluster based on dual processors Pentium III 1 GHz Intel computers (133 MHz bus), and a newer cluster based on dual Pentium Xeon 1.7 GHz Intel computers (400 MHz bus). The operating system environment and the software libraries there were used for this study are reported below:

- Linux (Debian 3.0),
- Kernel 2.4.18,
- gcc 2.95.4,
- MPI (lam-6.5.6),
- FFTW 2.1.3/P4FTTW-GEL-1.2.

6.1. Signal processing data flow

The detection software environment (Fig. 2) is composed by four main processes communicating through MPI calls:

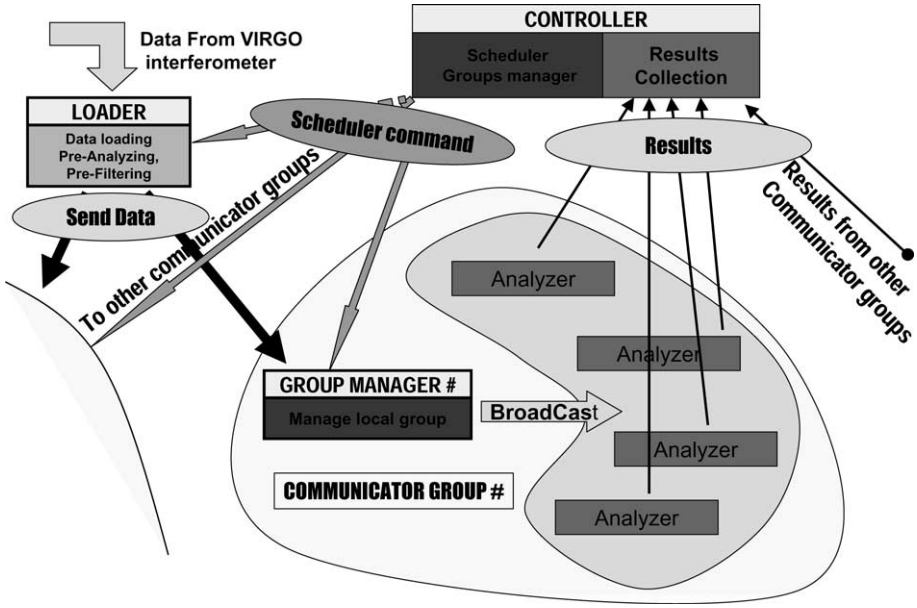

Fig. 2. Distributed program scheme.

Table 1
STREAM benchmarks on different CPU types: in the cells are reported the performance index in Megabytes per second and, between parentheses, the increment factor respect the Pentium-III CPU

CPU type	PIII 1 GHz SDRAM 133 MHz	AMD Athlon 1.2 GHz DDR 266 MHz	Xeon 1.7 GHz RDRAM 400 MHz
Copy $a[i] = b[i]$	363 (1)	888 (2.4)	1435 (3.9)
Scale $a[i] = \alpha \cdot b[i]$	363 (1)	571 (1.5)	1435 (3.9)
Add $a[i] = b[i] + c[i]$	461 (1)	1000 (2.2)	1600 (3.4)
Triad $a[i] = b[i] + \alpha \cdot c[i]$	400 (1)	705 (1.7)	1600 (4.0)

- **Controller**: one process for the whole cluster.
- **Loader**: one process for the whole cluster.
- **Group Manager**: one or more processes (one for each active master in the cluster).
- **Analyzer**: one or more processes for each Group Manager.

Data are read from the Virgo data stream (currently from disk storage) by the Loader process. This process is responsible also for signal conditioning (i.e. whitening [19]) and pre-analysis (i.e. data quality vetoing). Here the time series coming from the interferometer is downsampled and transformed into the frequency domain by means of a Fast Fourier Transform. The output of the Loader module is sent to a Group Manager, that dispatches it to the Analyzer processes belonging to the same MPI communicator. Each Analyzer process is responsible for a predetermined set of templates, kept in physical memory (RAM), against which the signal is matched. The output of the Wiener filters computed by the Analyzer processes are sent to the Controller process. This process regulates the data fluxes and provides continuous access to the results of the above signal processing chain.

7. Filtering performance

For performance reasons, the templates used for matched filtering are kept in RAM memory. Thus, the performance of the data processing scheme outlined in the previous section is heavily dependent on memory bandwidth, in addition to the obvious dependence on CPU speed. As mentioned above, two different PC architectures have been evaluated as part of this study: a cluster of dual-CPU Pentium-III machines, and a cluster of dual-CPU Xeon nodes. To estimate *a priori* the expected difference in performances between the Pentium-III CPUs and the Xeon CPUs, measures were taken (see Table 1) using the STREAM benchmark (http://www.streambench.org/). It is clear that the performance increase for Xeon-based nodes is mainly due to BUS clock (ratio $1 : 2 : 3$) rather than to simple CPU clock ($1 : 1.2 : 1.7$). The promised performance gain of RamBus technology is not easily spotted in the complex scenario of matched filtering. The matched filter can be seen as composed of three main steps:

- Array product,
- Inverse real Fourier transform (rFFT),
- Detection of the largest peak in an array of data (*max. detection*).

In the first two data rows of Table 2, the contributions of each of the above steps to the overall computation time is reported for the two node types. An overall performance gain of only 1.3 ($= 238/181$) can be observed, together with an abnormal weight of the FFT computation time.

7.1. Dual processors machines

All the nodes used for testing were dual processor machines. This choice optimizes cost, but can reduce the overall performance. In fact, concurrent access of the two CPUs to memory can cause bus contention and

Table 2
Total computation time and single contributions in the matched filter implementation

	Total time (ms)	Array product	rFFT	Max detection
PIII	238	13.4%	75.3%	11.3%
Xeon	181	4.1%	94.8%	1.1%
Xeon (P4FFTW-GEL)	106	8.0%	88.0%	4.0%

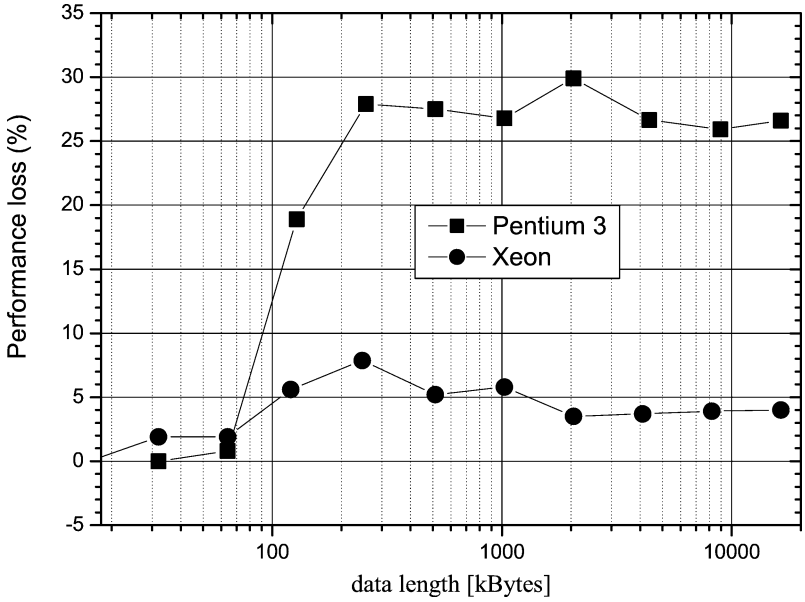

Fig. 3. Loss of performance (in percentage) for FFT computation in a dual processor machine with respect to a single processor (same CPU) machine. Intel Pentium III are indicated with a full square and Intel Xeon with a full circle.

thus degraded performance of the filtering processes. This is shown in Fig. 3, where the loss of performance in FFT computation is reported versus the data buffer length. It is evident that the 400 MHz bus clock of the Xeon machines partially mitigates this performance issue.

7.2. Dimensioning the Beowulf cluster

From Fig. 4, it is possible to extract the number of templates that each Xeon-based node is able to compute in the current configuration: with a data buffer of 4 MB, a single processor machine is able to compute about 5.5 templates per second (less than 5 templates per second and per CPU in a dual processor configuration, with a relative loss of about 12%). In 150 seconds, each node is able to evaluate 825 templates (726 per CPU in a dual configuration), so that about 55÷62 Xeon CPUs are needed to evaluate the whole template grid. Each node must have at least 4 GB of RAM (8 GB in case of dual processor nodes).

It has already been noticed (see Table 2) that the performance increase found for Xeon CPUs is lower than expected. From Figs. 3 and 4 it is apparent that a huge performance drop occurs when the data length overcomes about 200 kB. This is related to level-2 cache size (256 kB) of the Xeon processors used for this test. Since the Xeon CPU has a Pentium 4 core, an experimental version of FFTW with Pentium 4 optimizations (P4FFTW-GEL, see http://www.fftw.org) was also tested. In this case a large performance gain was observed, as reported in the last row of Table 2 and in Fig. 5 (where the knee at about 256 kB has also

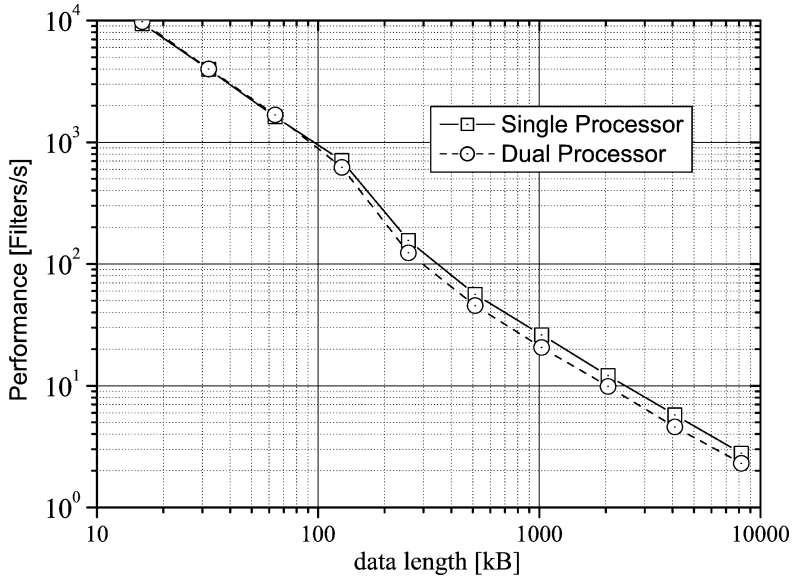

Fig. 4. Number of computed templates per second, in a dual Xeon processor machine (empty circle symbol, dashed line) and in a single processor identical machine (empty square symbol, continuous line).

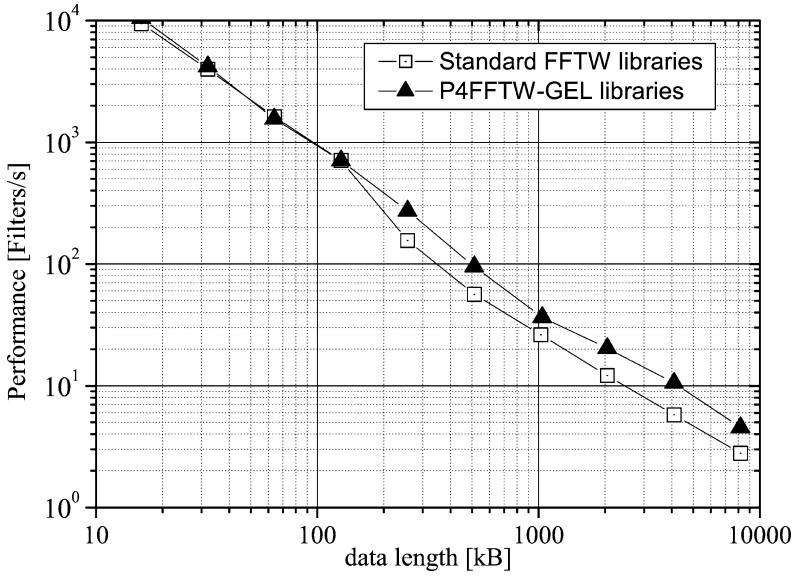

Fig. 5. Comparison of the matched filtering performance (in a single Xeon processor machine) using the standard FTTW (empty square symbol) or the Pentium 4 optimized p4fftw-gel libraries (full triangle symbol).

vanished) and the number of templates that each CPU is able to compute, per second, is about 10; this means that, by using these libraries, it should be possible to match 45,000 templates with 30 Xeon CPUs (8 GB RAM each).

8. Network performance

The results obtained in Section 7.2 assume that a perfectly linear scaling occurs when increasing the number of CPUs involved in the data analysis. The

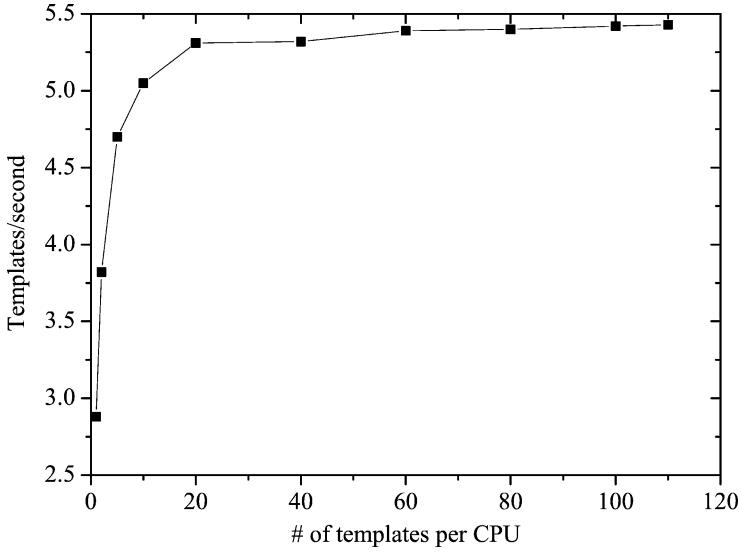

Fig. 6. Intensive matched filtering test on a small scale prototype based on Xeon CPUs and standard FFTW libraries.

data stream coming out of the interferometer undergoes a signal conditioning phase (prefiltering, whitening, vetoing) and then a forward Fourier transform is performed on the front-end machine, namely the *master* of the cluster. Data are then dispatched to all the nodes in the Beowulf cluster. Data communication is performed through MPI calls (see http://www.lam-mpi.org) on a fully switched Gigabit network. Taking in account the overhead due to MPI and TCP/IP, the effective transfer rate of this network is about 300 Megabit per second. This means that about 110 ms are needed to transfer the data buffer to a single Beowulf node. For 60 nodes, the full transfer time, using a sequential MPI_Send loop, is lower than 7 seconds and it is less than 5% of the time window available to compute all the filters. By using a MPI_Bcast call, the time needed to send data to N nodes scales as $\log_2 N$, rather than N. For 60 nodes, less than one second is needed to transfer the data stream to all the nodes, and a fully synchronous approach to coding can be adopted [20], greatly simplifying the data flow and software design.

9. Small-scale prototype

A small-scale software detection prototype was implemented using 8 dual-processor Xeon machines connected through a fully-switched Gigabit network. To avoid bus contention and make the performance analysis easier, one of the two processors in each machine has been left idle while the other was performing matched filtering. Standard FFTW libraries have been used. Results are reported in Fig. 6, where it is clear a plateau of 5.5 templates per second is already reached with a number of templates per CPU lower than the 825 required in the full scale computation. The performance loss shown for few templates per CPU is due to the relative importance of communication overheads in those conditions.

10. Conclusions

The feasibility of an *in-time* detection system for coalescing binaries signal in the Virgo interferometric gravitational wave detector has been demonstrated. A middle-scale Beowulf cluster of Intel Pentium Xeon processors was proposed, running an MPI-based parallel matched filtering software. In this configuration, to detect stars whose mass ranges from 0.9 to 2.0 solar masses, a cluster with about 60 Xeon CPUs is required. To include more massive binary systems (massive neutron stars or black holes) in the detection, a larger cluster is needed, but the shorter length of the corresponding templates reduces the additional computational requirements. Much larger computational

power is expected to be needed if the star spin is included in the template construction [21].

Acknowledgements

This research has been supported by the Istituto Nazionale di Fisica Nucleare (INFN) under the Virgo Project.

References

[1] J.H. Taylor, et al., Nature 355 (1992) 132.
[2] J. Weber, Phys. Rev. 355 (1960) 306.
[3] E. Coccia, Physica B 280 (2000) 525.
[4] A. Abramovici, et al., Science 256 (1992) 325.
[5] K. Danzmann, et al., GEO600: Proposal for a 600 m Laser Interferometric Gravitational Wave Antenna, Max-Planck-Institut für Quantenoptik Report 190, Garching, Germany, 1994.
[6] K. Tsubono, the TAMA collaboration, in: K. Tsubono, M.-K. Fujimoto, K. Kuroda (Eds.), Gravitational Wave Detection, Universal Academy Press, 1997.
[7] A. Giazotto, Phys. Rep. C 182 (1989) 365.
[8] E. Bougleux, et al., Nucl. Instr. Methods Phys. Res. A 409 (1988) 480.
[9] G. Cagnoli, et al., Phys. Lett. A 255 (1999) 230.
[10] M. Punturo, The VIRGO sensitivity curve, VIR-NOT-PER-1390-51, Virgo Internal Note, 2001, and see http://www.virgo.infn.it/senscurve/.
[11] M. Davier, Nucl. Phys. B (Proc. Suppl.) 87 (2000) 453.
[12] A. Einstein, et al., Ann. Math. 39 (1938) 65.
[13] L. Blanchet, et al., Phys. Rev. D 58 (1998) 124002.
[14] L. Blanchet, et al., Phys. Lett. A 271 (2000) 58.
[15] A. Papoulis, Probability, Random Variables and Stochastic Processes, McGraw-Hill, 1984.
[16] P. Canitrot, et al., Computational costs for coalescing binaries detection in VIRGO using matched filters, VIR-NOT-PIS-1390-149, Virgo Internal Note, 2000.
[17] M. Luise, G.M. Vitetta, Teoria dei Segnali, McGraw-Hill, 1999.
[18] S.M. Kay, Fundamentals of Statistical Signal Processing, in: Signal Processing Series, Prentice-Hall, 1998.
[19] E. Cuoco, et al., Class. Quant. Grav. 18 (2001) 1727.
[20] L. Bosi, M. Punturo, Performance test on the Small Scale Facility in Cascina for the Coalescing Binaries detection, VIR-NOT-PER-1390-223, Virgo Internal Note, 2002.
[21] P. Grandclment, et al., gr-qc/0207062, 16 Jul. 2002.